Research Article | Vol. 28, No. 3 / 3 February 2020 / Optics Express 2828
Optics EXPRESS

Self-healing properties of Hermite-Gaussian correlated Schell-model beams

ZHIHENG XU,[1,2] XIANLONG LIU,[1,2] YAHONG CHEN,[3] FEI WANG,[3] LIN LIU,[3,6] YASHAR E. MONFARED,[5] SERGEY A. PONOMARENKO,[4,5] YANGJIAN CAI,[1,2,3,7] AND CHUNHAO LIANG[1,2,8]

[1]*Shandong Provincial Engineering and Technical Center of Light Manipulations & Shandong Provincial Key Laboratory of Optics and Photonic Device, School of Physics and Electronics, Shandong Normal University, Jinan 250014, China*
[2]*Collaborative Innovation Center of Light Manipulations and Applications, Shandong Normal University, Jinan 250358, China*
[3]*School of Physical Science and Technology, Soochow University, Suzhou 215006, China*
[4]*Department of Electrical and Computer Engineering, Dalhousie University, Halifax, Nova Scotia B3J2X4, Canada*
[5]*Department of Physics and Atmospheric Science, Dalhousie University, Halifax, Nova Scotia B3J2X4, Canada*
[6]*liulin@suda.edu.cn*
[7]*yangjiancai@suda.edu.cn*
[8]*cliang@dal.ca*

Abstract: We study theoretically and experimentally the influence of the obstacle position separation from the source on the self-healing capacity of partially coherent beams using Hermite-Gaussian correlated Schell-model beams as a case in point. We establish that the shorter the distance between the obstacle and the source plane and the longer the distance between the obstacle and the observation (receiver) plane, the better the self-healing capacity of the beams. In addition, a similarity degree between the reconstructed and original beams is introduced to quantify the self-healing capacity of partially coherent beams. The derived interesting results may find applications in optical information processing, image transmission, and recovery.

1. Introduction

Self-healing refers to the phenomenon of beam reconstructing its source intensity profile at a distance past an opaque obstacle. The study of this phenomenon was triggered by research on diffraction-free optical beams such as Bessel, Airy beams [1–6], etc. As has been verified by experiments, nearly non-diffracting beams, which are finite aperture realizations of the ideal non-diffracting beams, display the remarkable property of self-reconstruction on free space propagation [5,7]. More importantly, this class of beams can also maintain its self-healing capacity in nonlinear, scattering turbid and/or random media, paving the way to attractive applications for human tissue microscopy and optical tweezers [5,8,9], among others. To date, a variety of diffraction-free beams, including optical ring lattices [10], Pearcey beams [11], optical pillar arrays [12], and dark and anti-dark diffraction free beams [13,14], have been generated and their self-healing properties have been verified. Despite a variety of intensity shapes of self-healing beams, at the fundamental level, self-healing can be explained in terms of the beam Poynting vector behavior [5,10,12].

To generate partially coherent beams, one way is to degrade spatial coherence of fully coherent laser beams by transmitting such beams through a rotating ground glass diffuser, for example [15]. The beam degree of spatial coherence in general, and the coherence width of statistically

#383805 https://doi.org/10.1364/OE.383805
Journal © 2020 Received 22 Nov 2019; revised 24 Dec 2019; accepted 24 Dec 2019; published 10 Jan 2020

Optics EXPRESS

homogeneous beams in particular, provide an important degree of freedom to control the spatial profile and polarization of light beams. The partially coherent beams have found various important applications in many areas [16–18]. In 2016, Wang etc. introduced the concept of self-reconstruction for partially coherent beams [18]. The most significant conclusion of this research was that the self-reconstruction ability of any partially coherent beam, regardless of its spatial profile, is independent of the obstacle shape provided that the beam coherence area is well below the transparent area of the obstacle. To follow up on this work, Wu et al., [19] examined self-healing properties of generic statistically homogenous (Schell-model) type of beams [15]. However, the results of [15,18,19] are limited to the obstacles located in the source plane.

In this work, we examine the impact of the obstacle position and the receiver plane position on the self-healing capacity of Schell-model partially coherent beams. Specifically, we study the effect of the obstacle position and the receiver plane position on the self-healing capacity of Hermite-Gaussian correlated Schell-model (HGCSM) beams. They are known for their ability to split into two or four beamlets with nonzero beam order on free space propagation due to the structure of their spatial degree of coherence at the source. Further, this self-splitting property is more pronounced for higher order beams [20]. We show numerically and verify experimentally that even for an obstacle with the opaque angle of $3\pi/2$, the scattered beam can retain its splitting spatial profile upon the suitable positions of the obstacle and the receiver. In addition, we quantified the self-healing capacity of the beam by introducing a modified similarity degree between the reconstructed and original beams.

2. Theory and numerical simulations

In the space-frequency domain, the second-order statistical properties of partially coherent sources can be described in terms of their cross-spectral density (CSD) functions at a pair of points in space. The CSD function of a HGCSM source reads [20]

$$W_s(\boldsymbol{\rho}_1, \boldsymbol{\rho}_2) = G_0 \exp\left[-\frac{\boldsymbol{\rho}_1^2 + \boldsymbol{\rho}_2^2}{4\sigma_0^2}\right] \gamma(\boldsymbol{\rho}_2 - \boldsymbol{\rho}_1). \tag{1}$$

Here $\boldsymbol{\rho}_1$, $\boldsymbol{\rho}_2$ are two arbitrary points in the source plane, G_0 is a constant, σ_0 is the beam waist width at the source; $\gamma(\boldsymbol{\rho}_2 - \boldsymbol{\rho}_1)$ denotes the spectral degree of coherence (DOC), which is given by [20]

$$\begin{aligned}\gamma(\boldsymbol{\rho}_2 - \boldsymbol{\rho}_1) = &\frac{H_{2m}[(x_2-x_1)/\sqrt{2}\delta_{0x}]}{H_{2m}(0)} \exp\left[-\frac{(x_2-x_1)^2}{2\delta_{0x}^2}\right] \\ &\times \frac{H_{2n}[(y_2-y_1)/\sqrt{2}\delta_{0y}]}{H_{2n}(0)} \exp\left[-\frac{(y_2-y_1)^2}{2\delta_{0y}^2}\right].\end{aligned} \tag{2}$$

In Eq. (2), H_{2m} and H_{2n} are the Hermite polynomials of the order m and n, respectively; δ_{0x} and δ_{0y} denote the transverse coherence widths along the x and y directions, respectively.

In Fig. 1, we display an HGCSM beam scattered by an opaque obstacle propagates toward a receiver plane. The distances from the source plane to the obstacle and receiver planes are L and D, respectively. The CSD of such beams in the front surface of the obstacle plane can be expressed using the Huygens-Fresnel diffraction integral [21] as

$$W_b(\mathbf{r}_2, \mathbf{r}_1) = \frac{e^{ikL}}{i\lambda L} \int_{-\infty}^{\infty}\int_{-\infty}^{\infty} W_s(\boldsymbol{\rho}_2, \boldsymbol{\rho}_1) e^{i\frac{k}{2L}(\mathbf{r}_2^2 + \mathbf{r}_1^2 - \boldsymbol{\rho}_2^2 - \boldsymbol{\rho}_1^2)} d^2\boldsymbol{\rho}_1 d^2\boldsymbol{\rho}_2, \tag{3}$$

where λ is the wavelength of light and $k = 2\pi / \lambda$ stands for the wavenumber. The CSD of the beam right past the obstacle can be expressed as

$$W_o(\mathbf{r}_2, \mathbf{r}_1) = R(\mathbf{r}_1) R^*(\mathbf{r}_2) W_b(\mathbf{r}_2, \mathbf{r}_1), \tag{4}$$

Optics EXPRESS

where $R(\mathbf{r})$ is the transmission function of the opaque obstacle. The CSD of such beam in the receiver plane can then be written as

$$W_r(\mathbf{v}_2, \mathbf{v}_1) = \frac{e^{ik(D-L)}}{i\lambda(D-L)} \int_{-\infty}^{\infty}\int_{-\infty}^{\infty} W_o(\mathbf{r}_2, \mathbf{r}_1) e^{i\frac{k}{2(D-L)}(\mathbf{v}_2^2+\mathbf{v}_1^2-\mathbf{r}_2^2-\mathbf{r}_1^2)} d^2\mathbf{r}_1 d^2\mathbf{r}_2, \tag{5}$$

where $\mathbf{v}_1$ and $\mathbf{v}_2$ are the transverse position vectors in the receiver plane. The average intensity in the receiver plane follows at once from Eq. (5) to be

$$I(\mathbf{v}) = W_r(\mathbf{v}, \mathbf{v}). \tag{6}$$

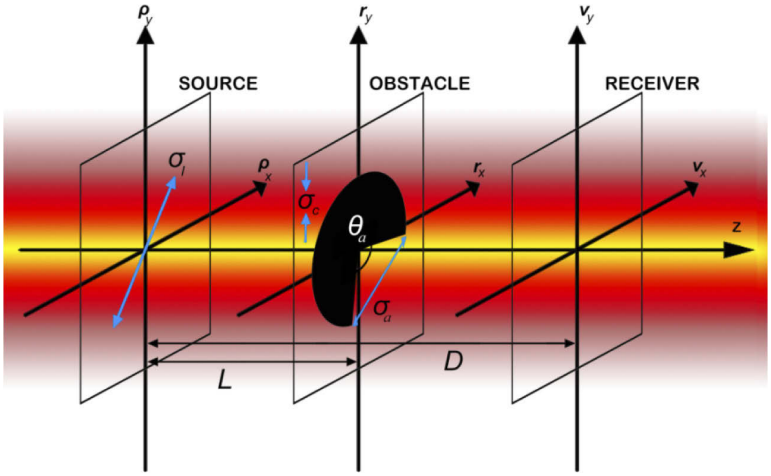

Fig. 1. Illustrating the system geometry. The distances from the source plane to the obstacle and receiver planes are L and D, respectively.

The self-healing ability of a partially coherent beam is associated with an obstacle dimension. The partially coherent beam self-healing can be realized well if the source coherence area S_c, the transparent area of an obstacle S_a and the beam intensity cross-section area S_I satisfy the following condition [18]

$$S_I > S_a \gg S_c. \tag{7}$$

In the following numerical example, the transparent section of the obstacle is a quarter of the beam spot area. The transverse coherence width and beam width of the HGCSM beam are set to $\delta_{0x} = \delta_{0y} = 0.2$ mm, and $\sigma_0 = 1$ mm, respectively, which satisfies the inequality Eq. (7). The order of the Hermite polynomial is set to be $m = n = 4$ and the wavelength λ is given by 632.8 nm.

To illustrate the effect of the obstacle location on the beam self-healing capacity, we adjust the distance L (Fig. 1) between the source plane and the obstacle, while keeping the distance D (Fig. 1) between the source and receiver planes fixed. In Fig. 2, for the first panel row, we show the intensity distributions of an HGCSM beam propagating in free space without any obstacles from the source ($D = 0$ mm) to $D = 190$ mm. The intensity profile of the beam is expected to split into four beamlets [20]. In Fig. 2(f), we visualize the transmission function of the obstacle plane with the transparent section indicated in white: Only a quarter of the obstacle plane is transparent, and the other black area is opaque. Next, we demonstrate the effect of the obstacle position on the beam self-healing capacity. First, we set the location of the obstacle to $L = 70$, 110, 150, 190 mm, respectively. In Figs. 2(g)– 2(j), we display the intensity distributions of

Optics EXPRESS

the scattered beam in the receiver plane, placed right after the obstacle plane, namely $D = L$. In Figs. 2(l)– 2(o), we exhibit the receiver plane intensity distributions of the HGCSM beam scattered by the obstacle that is located at the indicated distance L. In addition, we present the free propagating HGCSM beam intensity distribution in the receiver plane in Fig. 2(k) as a reference. Our simulation results indicate that whenever the receiver plane is fixed, the beam self-healing capacity decreases with the distance between the source and the obstacle. At the same time, if the HGCSM beam propagates over the distance from the source longer than 190 mm, it splits into four beamlets and entirely loses any ability to self-heal.

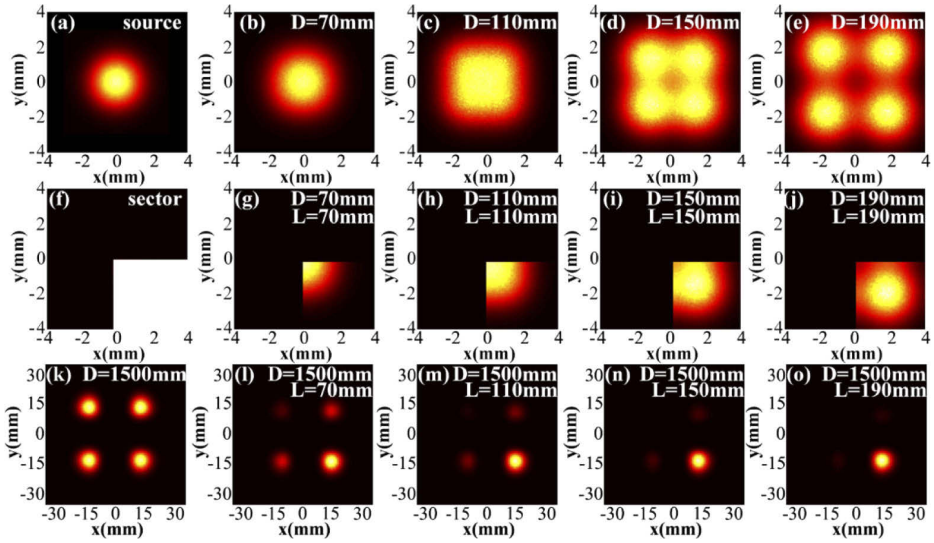

Fig. 2. Intensity distributions of an HGCSM beam, scattered by an opaque obstacle located at a distance L away from the source, in the receiver plane located at a distance D away from the source: (a - e) the intensity distributions of an HGCSM beam on propagation without the obstacle; (f) two-dimensional distribution of the obstacle transmittance; (g - j) the intensity distributions of an HGCSM beam in the receiver plane right after the obstacle (i.e., $L = D$); (k) the intensity distributions of an HGSCM beam propagated to $D = 1500$ mm without the obstacle; (l - o) The intensity distributions of an HGCSM beam propagated to $D = 1500$ mm, who is scattered by the obstacle located at $L = 70$, 110, 150, 190 mm, respectively.

Next, we study the effect of the receiver plane location on the beam self-healing capacity. To this end, we consider an obstacle fixed at $L = 70$ mm from the source plane and display in Figs. 3(a)–3(e) the intensity distributions of the scattered HGCSM beam at several propagation distances. As we can infer from the first panel row of Fig. 3, the scattered beam splits right after the obstacle plane and reconstructs its intensity profile gradually as the beam propagates away from the obstacle. Our simulations indicate that the four-beamlet structure of the beam does not change past the plane $D = 1500$ mm. We can readily infer form Fig. 3(e) that the beam can self-reconstruct, though the intensity of some beamlets is somewhat weak. As was discussed at length in [22,23], the low-coherent beam intensity distributions in the free space are mainly controlled by the source degree of coherence which is defined as a normalized second-order correlation function of the beam fields at a pair of spatial points in the source plane [21,24]. We then briefly discuss the degree of coherence of the HGCSM beams scattered by the obstacle. In the second and third panel rows in Fig. 3, we display the HGCSM beam the square of the modulus of the degree of coherence evolution without and with the obstacle (located at

Optics EXPRESS

$L = 70$ mm), respectively. We find that the obstacle has virtually no effect on the degree of coherence distribution, implying that the latter is immune to the obstacle presence. These results may find applications to image transmission with partially coherent light through turbid media.

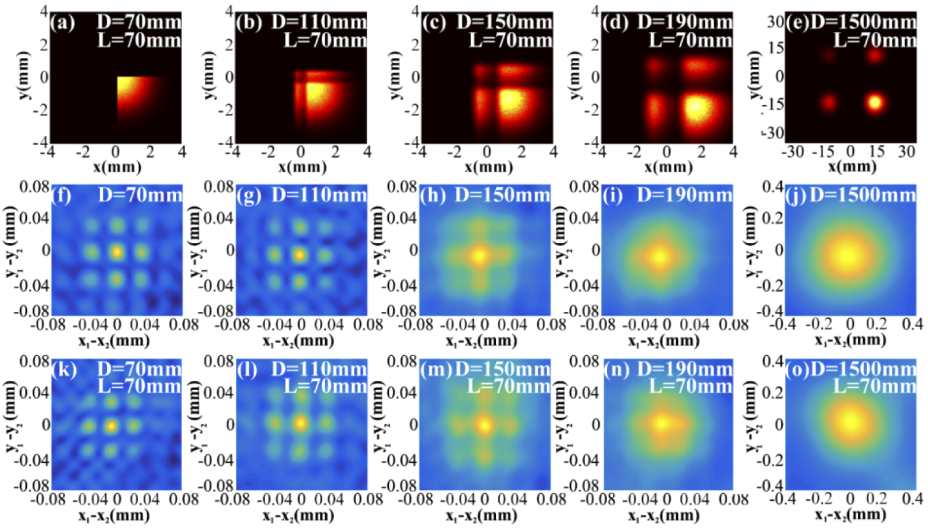

Fig. 3. Self-healing process of an HGCSM beam scattered by the obstacle located at $L = 70$ mm from the source plane: (a - e) intensity distributions of such scattered beams propagated to different distances; (f - j) the square of the modulus of the degree of coherence distributions of the HGCSM beams propagated to different distance without an obstacle; (k - o) the square of the modulus of the degree of coherence distributions of such beams propagating to the different distances, scattered by an obstacle at $L = 70$ mm.

In order to quantify the influence of the obstacle position and receiver plane position on the self-healing capacity of the beam, we suggest a new self-healing similarity degree as

$$D_p(z) = \frac{\left[\iint \langle I_{wt}(\boldsymbol{\rho}, z)\rangle \langle I_{ob}(\boldsymbol{\rho}, z)\rangle \, d^2\boldsymbol{\rho}\right]^2}{\iint \langle I_{wt}(\boldsymbol{\rho}, z)\rangle^2 d^2\boldsymbol{\rho} \iint \langle I_{ob}(\boldsymbol{\rho}, z)\rangle^2 d^2\boldsymbol{\rho}}, \tag{8}$$

where the angular brackets denote ensemble averaging; I_{wt} and I_{ob} stand for the beam intensities without and with obstruction, respectively. In contrast to the similarity degree definitions put forward elsewhere [8,18,25,26], our definition addresses the following aspects. First, the area of integration in Eq. (8) is extended over the whole transverse plane. Second, the similarity degree varies from zero to unity, zero representing lack of any similarity and unity representing complete identity of I_{wt} and I_{ob}.

In Fig. 4, we display the similarity degree of the scattered beam versus L and D. We first observe in Fig. 4(a) that as the receiver plane position is fixed at $D = 1500$ mm, the magnitude of the similarity degree decreases with the distance L between the obstacle and the source plane. Instructively, even if the obstacle is placed at the source plane ($L = 0$ mm), the similarity degree may not reach unity in the receiver plane. Second, in Fig. 4(b) we exhibit the similarity degree as a function of the receiver plane position D for several values of L, $L = 30$, 70, 150 mm. We can infer from the figure that the shorter the distance L between the source and the obstacle, or the longer the distance D between the obstacle and the receiver plane, the better the beam self-healing capacity.

Optics EXPRESS

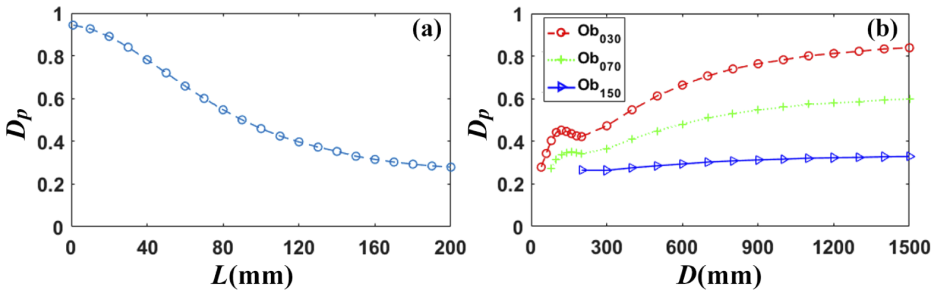

Fig. 4. Similarity degree as a function of the obstacle L and receiver plane D positions: (a) similarity degree as a function of L with $D = 1500$ mm; (b) similarity degree as a function of D with $L = 30$ mm (in red), 70 mm (in green) and 150 mm (in blue), respectively.

3. Experimental results

We now describe the HGCSM beam generation and verification of our theoretical results on beam self-healing.

In Fig. 5, a fully coherent quasi-monochromatic beam with the carrier wavelength $\lambda = 632.8$ nm, generated by a He-Ne laser, was expanded by a beam expander (BE), followed by passing through a spatial light modulator (SLM), pre-loaded with a designed hologram that determines the beam order of the generated HGCSM beam [19,20]. The first-order of the diffracted beam was selected by a circular aperture (CE) and the mirrors M_1 and M_2 directed the beam towards a lens L. After focused by the lens L, the beam passed through a rotating ground glass disk (RGGD) and then an incoherent beam was produced. Next, the generated incoherent beam was transmitted through a lens L_1 and a Gaussian amplitude filter (GAF) located at $z = 0$ mm, resulting in the HGCSM beam generation. By adjusting the distance between the lens L and RGGD, we are able to control the coherence widths δ_{0x}, δ_{0y} of the HGCSM beam. The generated HGCSM beam, scattered by

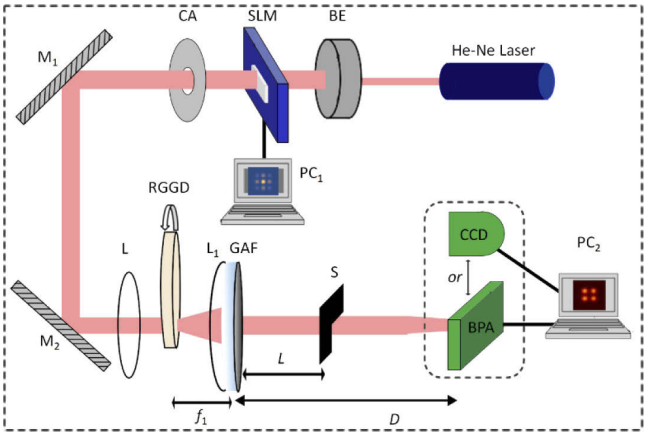

Fig. 5. Experimental setup for producing an HGCSM beam and measuring the beam self-healing properties of the scattered HGCSM beam. BE, Beam expander; SLM, Spatial light modulator; CA, Circular aperture; M_1 and M_2, Reflecting mirror; L, L_1, L_2, L_3, Thin lenses; RGGD, Rotating ground glass disk; GAF, Gaussian amplitude filter; S, Obstacle; BS, Beam splitter; CCD, Charge coupled device; BPA, Beam profile analyzer.

Optics EXPRESS

an obstacle located at $z = L$, arrived at the receiver plane at $z = D$. In our experiment, we use a sheet of opaque paper as an obstacle. The thickness of the sheet is only about 0.3 mm such that the obstacle thickness effect on self-healing properties is negligible in this work. In the receiver plane, the beam profile analyzer (BPA) and the charge coupled device (CCD) are used to measure the intensity and the square of the modulus of the degree of coherence distributions as described in greater detail in a recent review [22].

In the first panel row of Fig. 6, we display the experimental results for the free-propagating (no obstacle) HGCSM intensity distributions. As evidenced by the figure, the initial Gaussian-like intensity profile splits into four beamlets. We also exhibit the measured intensity distributions of the HGCSM beam scattered by the obstacle at $L = 70$, 110, 150, 190 mm just after the obstacle (namely $D = L$) in the second panel row of Fig. 6. Meanwhile, the intensity distributions of such the scattered HGCSM beams in the receiver plane $D = 1500$ mm are given in the bottom panel row. We can conclude by comparing Figs. 2 and 6 that our experimental results validate our theoretical prediction that the self-healing ability of the beam degrades as the distance L increases, with the receiver plane position fixed. In addition, if the obstacle is located in the transverse plane where the beam intensity profile is split completely, the self-healing is almost impossible to occur, which is evidenced by comparing Figs. 6(d) and 6(l).

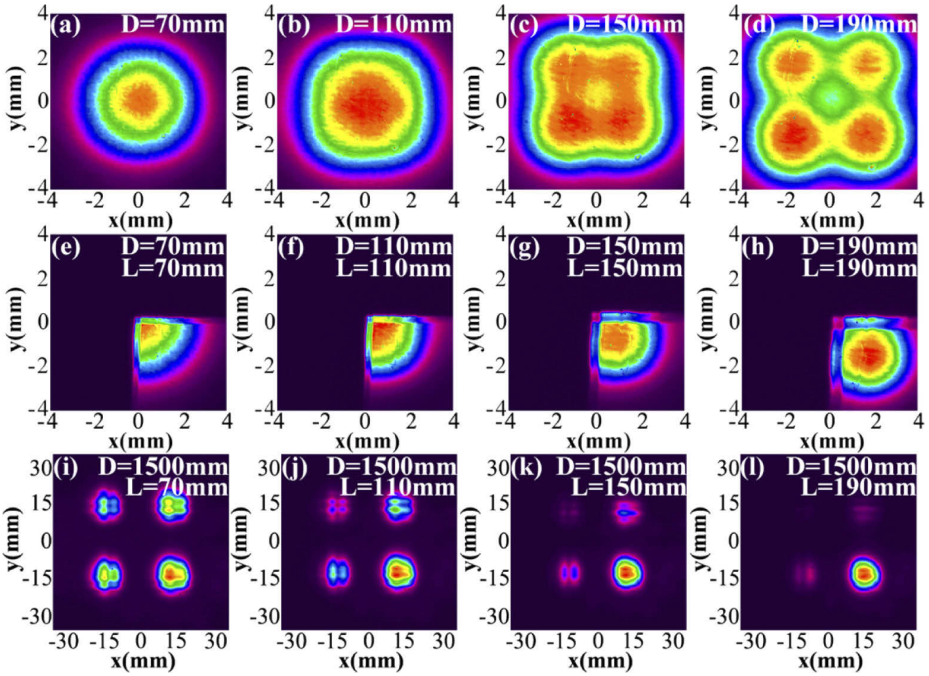

Fig. 6. Experimental results for the intensity distributions of an HGCSM beam on propagation with or without the opaque obstacle. (a - d) Experimental results for the intensity distributions of an HGCSM beam propagating to the different distances $D = 70$, 110, 150, 190 mm, respectively, without an obstacle; (e - f) Experimental results for the intensity distributions of an HGCSM beam in the receiver plane just after the opaque obstacle located at $L = 70$, 110, 150, 190 mm, respectively (i.e., $D = L$). (i - j) Experimental results for the intensity distributions of an HGCSM beam propagated to $D = 1500$ mm, scattered by an opaque obstacle located at $L = 70$, 110, 150, 190 mm, respectively.

Optics EXPRESS

In Fig. 7, we fix the opaque obstacle position at $L = 70$ mm and explore the reconstructed intensity and the square of the modulus of the degree of coherence distributions of the scattered HGCSM beam in the receiver plane, located at an adjustable distance D. We again find that the experimental results consistent with the theoretical anticipation shown in Fig. 3. In particular, the scattered HGCSM beam intensity distribution manifests a four-beamlet pattern which self-reconstructs upon the beam propagation away from the obstacle. At the same time, the HGCSM beam degree of coherence remains virtually unaffected by the obstacle.

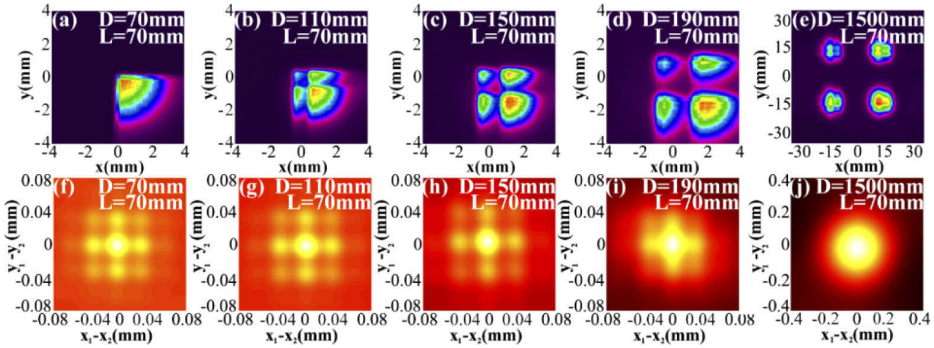

Fig. 7. Experimental results for the self-healing process of an HGCSM beam scattered by the obstacle located at $L = 70$ mm from the source plane. The intensity distributions shown in first panel row and the square of the modulus of the degree of coherence distributions shown in second panel row of such scattered HGCSM beam in the receiver plane at $D = 70$, 110, 150, 190 and 1500 mm, respectively.

Finally, we experimentally study the beam self-healing capacity as a function of the obstacle location and compare our results with the theory using the similarity degree concept. Specifically, we fix the receiver plane at $D = 1500$ mm, and vary the obstacle location L to study the beam self-healing capacity. We assume L to be in the range from 70 mm to 200 mm. The numerical and experimental results, given in Fig. 8, are shown in blue and red, respectively. As expected, the figure illustrates that the similarity degree decreases with the obstacle separation from the source L, implying the reduction of beam self-healing capacity. The experimental results are consistent with numerical simulations. The slight difference between the two is due to the experimental errors encountered as one tries to accurately determine the beam intensity distribution past the rotating ground glass disk.

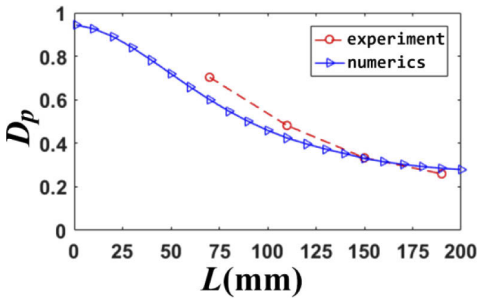

Fig. 8. Experimental results for the similarity degree of a scattered HGCSM beam propagated to $D = 1500$ mm as a function of the obstacle position L separation from the source plane.

Optics EXPRESS

4. Conclusions

In this work, we demonstrated, both numerically and experimentally, the influence of the opaque obstacle and receiver plane positions on the self-healing capacity of HGCSM beams. We have found that the shorter the distance between the obstacle and the source plane—or the longer the distance between the obstacle and the receiver plane—the better the beam self-healing capacity. By the same token, we have demonstrated that if the obstacle is located in the transverse plane where an HGCSM beam is completely split, complete self-healing cannot be realized. At the same time, we have shown that the beam degree of spatial coherence structure is immune to the obstacle. In addition, we introduced a similarity degree to quantify the beam self-healing capacity. Finally, to validate our theoretical anticipations, we carried out the experiment. We have found our experimental results consistent with our simulations. Our results are anticipated to find applications to optical information processing, image transmission, and recovery.

Funding

Natural Sciences and Engineering Research Council of Canada (RGPIN-2018-05497); National Natural Science Foundation of China (11525418, 11774251, 11804198, 11874046, 11947239, 11974218, 91750201); China Postdoctoral Science Foundation (2019M662424); Innovation Group of Jinan(2018GXRC010).

Acknowledgments

We thank Baoxin Qi for useful discussions.

References

1. S. Sogomonian, S. Klewitz, and S. Herminghaus, "Self-reconstruction of a Bessel beam in a nonlinear medium," Opt. Commun. **139**(4-6), 313–319 (1997).
2. Z. Bouchal, J. Wagner, and M. Chlup, "Self-reconstruction of a distorted nondiffracting beam," Opt. Commun. **151**(4-6), 207–211 (1998).
3. Z. Bouchal and J. Wagner, "Self-reconstruction effect in free propagation of wavefield," Opt. Commun. **176**(4-6), 299–307 (2000).
4. P. Fischer, H. Little, R. Smith, C. Lopez-Mariscal, C. Brown, W. Sibbett, and K. Dholakia, "Wavelength dependent propagation and reconstruction of white light Bessel beams," J. Opt. A: Pure Appl. Opt. **8**(5), 477–482 (2006).
5. J. Broky, G. Siviloglou, A. Dogariu, and D. Christodoulides, "Self-healing properties of optical Airy beams," Opt. Express **16**(17), 12880–12891 (2008).
6. X. Chu, G. Zhou, and R. Chen, "Analytical study of the self-healing properties of Airy beams," Phys. Rev. A **85**(1), 013815 (2012).
7. R. Herman and T. Wiggins, "Production and uses of diffractionless beams," J. Opt. Soc. Am. A **8**(6), 932–942 (1991).
8. F. Farrbach, P. Simon, and A. Rohrbach, "Microscopy with self-reconstructing beams," Nat. Photonics **4**(11), 780–785 (2010).
9. V. Garces-Chavez, D. McGloin, H. Melville, W. Sibbett, and K. Dholakia, "Simultaneous micromanipulation in multiple planes using a self-reconstructing light beam," Nature **419**(6903), 145–147 (2002).
10. P. Vaity and R. Singh, "Self-healing properties of optical ring lattice," Opt. Lett. **36**(15), 2994–2996 (2011).
11. J. Ring, J. Lindberg, A. Mourka, M. Mazilu, K. Dholakia, and M. Dennis, "Auto-focusing and self-healing of Pearcey beams," Opt. Express **20**(17), 18955–18966 (2012).
12. R. Cao, Y. Hua, C. Min, S. Zhu, and X. Yuan, "Self-healing optical pillar array," Opt. Lett. **37**(17), 3540–3542 (2012).
13. S. A. Ponomarenko, W. Huang, and M. Cada, "Dark and antidark diffraction-free beams," Opt. Lett. **32**(17), 2508–2510 (2007).
14. X. Zhu, F. Wang, C. Zhao, Y. Cai, and S. A. Ponomarenko, "Experimental realization of dark and antidark diffraction-free beams," Opt. Lett. **44**(9), 2260–2263 (2019).
15. Y. Cai, Y. Chen, J. Yu, X. Liu, and L. Liu, "Generation of partially coherent beams," Prog. Opt. **62**, 157–223 (2017).
16. X. Lu, Y. Shao, C. Zhao, K. Konijnenberg, X. Zhu, Y. Tang, Y. Cai, and H. Urbach, "Noniterative spatially partially coherent diffractive imaging using pinhole array mask," Adv. Photonics **1**(1), 016005 (2019).
17. P. Ma, B. Kacerovská, R. Khosravi, C. Liang, J. Zeng, X. Peng, C. Mi, Y. E. Monfared, Y. Zhang, F. Wang, and Y. Cai, "Numerical approach for studying the evolution of the degrees of coherence of partially coherent beams propagation through an ABCD optical system," Appl. Sci. **9**(10), 2084 (2019).

Optics EXPRESS

18. F. Wang, Y. Chen, X. Liu, Y. Cai, and S. Ponomarenko, "Self-reconstruction of partially coherent light beams scattered by opaque obstacles," Opt. Express **24**(21), 23735–23746 (2016).
19. G. Wu and X. Pang, "Self-Healing Properties of Partially Coherent Schell-Model Beams," IEEE Photonics J. **9**(6), 1–11 (2017).
20. Y. Chen, J. Gu, F. Wang, and Y. Cai, "Self-splitting properties of a Hermite-Gaussian correlated Schell-model beam," Phys. Rev. A **91**(1), 013823 (2015).
21. E. Wolf, *Introduction to the Theory of Coherence and Polarization of Light* (Cambridge University, 2007).
22. Y. Cai, Y. Chen, and F. Wang, "Generation and propagation of partially coherent beams with nonconventional correlation functions: a review [Invited]," J. Opt. Soc. Am. A **31**(9), 2083–2096 (2014).
23. C. Liang, R. Khosravi, X. Liang, B. Kacerovská, and Y. E. Monfared, "Standard and elegant higher-order Laguerre-Gaussian correlated Schell-model beams," J. Opt. **21**(8), 085607 (2019).
24. S. A. Ponomarenko and E. Wolf, "Coherence properties of light in Young's interference pattern formed with partially coherent light," Opt. Commun. **170**(1-3), 1–8 (1999).
25. A. Aiello, G. Agarwal, M. Paúr, B. Stoklasa, Z. Hradil, J. Řeháček, P. Hoz, G. Leuchs, and L. Sánchez-Soto, "Unraveling beam self-healing," Opt. Express **25**(16), 19147–19157 (2017).
26. X. Chu and W. Wen, "Quantitative description of the self-healing ability of a beam," Opt. Express **22**(6), 6899–6904 (2014).